Available online at www.sciencedirect.com
SCIENCE DIRECT®
International Journal of Heat and Mass Transfer 47 (2004) 287–305
International Journal of HEAT and MASS TRANSFER
www.elsevier.com/locate/ijhmt

Heat transfer in a swinging rectangular duct with two opposite walls roughened by 45° staggered ribs

S.W. Chang [a,*], L.M. Su [b], T.L. Yang [c]

[a] Department of Marine Engineering, National Kaohsiung Institute of Marine Technology, No. 142, Hai-Chuan Road, Nan-Tzu District, Kaohsiung 811, Taiwan, ROC
[b] Department of Electrical Engineering, Tung Fang College of Technology and Commerce, Kaohsiung 829, Taiwan, ROC
[c] Department of Electrical Engineering, Fortune Institute of Technology, Kaohsiung 842, Taiwan, ROC

Received 23 September 2002; received in revised form 18 June 2003

Abstract

This paper describes an experimental study of heat transfer in a rectangular channel with two opposite walls roughened by 45° staggered ribs swinging about two orthogonal axes under single and compound modes of pitching and rolling oscillations. A selection of heat transfer measurements illustrates the manner by which the swinging oscillations with and without buoyancy interaction modify local heat transfer along the centerline of rib-roughened surface in the range of 0.75–2.25 times of the static channel value. The compound rolling and pitching forces with harmonic and non-harmonic rhythms interacting with buoyancy exhibit synergistic effect to reduce heat transfer. An adverse buoyancy effect that reverses the buoyancy interaction from improving to impeding heat transfer when the relative strength of swinging force increases could develop in the channel that swings with compound mode oscillation. An empirical heat transfer correlation, which is physically consistent, has been developed that permits the individual and interactive effects of single and compound modes of swinging forces with and without buoyancy interaction on forced convection to be evaluated and quantified. This work has been motivated by the need to understand the general effect of swinging oscillation on the performance of the cooling passage in a rib-roughened plate-type heat exchanger under sea-going conditions.

Keywords: Pitching; Rolling; Rib-roughened channel; Heat transfer

1. Introduction

From the large-scale marine boiler to small-scale heat exchanger, heat transfer enhancement finds a wide range of applications in shipping machineries. In this respect, various types of surface ribs that provide heat transfer augmentation and generate complicated flow structures are often used to roughen the heated or cooled surfaces in a heat transfer device. These repeated surface ribs periodically break boundary layers of flow and promote turbulence; modify near-wall flow structure and/or induce cross-stream secondary flows in the flow passage, which in combination could considerably augment heat transfer. Although the heat transfer enhancement using surface ribs has been a subject of much fundamental research over the past years for static duct flow situations [1–5], only relatively few research efforts study the flow and heat transfer in the rib-roughened channels when the external force-field is present [6–9]. The effectiveness of these surface ribs on heat transfer augmentation varies with the geometrical features of the ribs, such as the height, pitch, angle of attack, orientation, shape and the manner of arrangement [1–5], and with the external force-field present, such as the centrifugal force in bend, Coriolis force in rotating channel and

* Corresponding author. Tel.: +86-886-7-810-0888x5216; fax: +86-886-7-5712219.
E-mail address: swchang@mail.nkimt.edu.tw (S.W. Chang).

0017-9310/$ - see front matter © 2003 Elsevier Ltd. All rights reserved.
doi:10.1016/S0017-9310(03)00411-3

Nomenclature

Bu	buoyancy parameter
A, B, C_s, F_s, G	coefficients
C_p	specific heat of fluid ($m^2 s^{-2} K^{-1}$)
D	hydraulic diameter of test duct (m)
f_P	pitching frequency (s^{-1})
f_R	rolling frequency (s^{-1})
H	swinging arm (m)
K	thermal conductivity of fluid ($W m^{-1} K^{-1}$)
Nu	swinging Nusselt number
Nu_0	stationary Nusselt number
Nu_∞	Nusselt number value for developed flow in plain empty tube
Pi	pitching number
Pr	Prandtl number
$\widetilde{P}$	dimensionless pressure of swinging flow
q_f	convective heat flux ($W m^{-2}$)
Re	Reynolds number
Ro	rolling number
T	fluid local temperature (K)
T_f	flow bulk temperature (K)
T_w	wall temperature (K)
$\widetilde{V}$	relative fluid velocity (ms^{-1})
W_m	mean through flow velocity (K)
x	axial location referred to $oxyz$ frame (m)
X	dimensionless axial location referred to $oxyz$ frame (z/d)
$\vec{i}$, $\vec{j}$, $\vec{k}$	unit vector of $oxyz$ reference frame
$oxyz$	swinging coordinate frame

Greek symbols

Ψ, ψ, φ	unknown functions
α	attack angle of ribs (deg)
β	thermal expansion coefficient of coolant (K^{-1})
Γ	dimensionless time scale ($\Omega_{R,P} \times t$)
Ω	angular velocity of swinging test duct (s^{-1})
η	dimensionless temperature
$\wp$	pitching function
$\Re$	rolling function
ξ, ζ	synergistic oscillation function
ν	fluid kinetic viscosity ($m^2 s^{-1}$)

Subscripts

P	pitching
R	rolling
0	reference condition

pulsating force in reciprocating duct [6–9]. The general rib-effects on heat transfer are the improved heat transmission and the complicated spatial heat transfer variations along the rib-roughened surface. Confident design tools for heat transfer prediction in the rib-roughened channel that are dominated by complex turbulent transport process are not yet available, especially when the enhanced channel periodically moves. It is a fact that ships roll, pitch and yaw when they navigate in the open sea. The frequencies of such swinging oscillations are low but the arms of swinging oscillations are on the order of 5–10 m for a merchandized vessel. In practice, the principal components of the overall transverse acceleration of a thermal-fluids device located on ship are gravity, tangential roll acceleration, and heave (pitch) acceleration. The distances of the thermal-fluids device from the center-gravity of the ship along with the sea-going conditions could change the magnitudes of pitching and rolling accelerations. Nevertheless, the classification society guidelines for maximum across-the-deck accelerations and normal-to-deck accelerations could be treated as the maximum lashing accelerations experienced by a sea-going ship. In this respect, the ABS lashing guidelines with maximum roll angle of 23.8° result the maximum across-the-deck and normal-to-deck accelerations in the ranges of 0.54–0.59 and 1.05–1.15 times of gravitational accelerations respectively. The present test program simulates the maximum rolling or pitching angle of 22.5° at the maximum swinging frequency of 1 Hz, which provides the maximum rolling and pitching accelerations of 0.15 and 0.3 times of gravitational acceleration respectively. This swinging condition simulated by the present study falls in the normal ranges of sea-going practices. Considerable influences of rolling and pitching motions on the thermo-fluids phenomena in a rib-enhanced channel could be resolved. Although the use of surface ribs has found a wide range of success for heat transfer augmentation [1–9], none of the past research efforts investigates the flow and heat transfer inside the rib-roughened channel that rolls or/and pitches, as with the application of plate-type heat exchanger in a ship. Note, for a rib-roughened plate-type heat exchanger, the width-to-gap ratio of its rectangular flow passage is in the typical range of 6–8, which configurations are rarely studied even if the channel remains stationary.

The lack of systematic research efforts to study the thermo-fluids science under the rolling or/and pitching environments, despite its wide applications for shipping machinery, is evident. There are few relevant studies demonstrating the modified flow and heat transfer phenomena in the swinging thermal-fluids system. As a result of swinging oscillations, heat transfer in a forced-convective swing swirl duct could be initially impaired from the static duct level, and then recovered when the relative strength of swinging forces increase that could

lead to heat transfer improvement form the static scenario. The synergistic effects of the harmonic and non-harmonic swinging oscillations in a swirl duct reduce heat transfer [10]. In a swinging closed cavity that is completely filled with liquid, the Stokes boundary layer arises near the cavity walls within which the vorticity is generated. The vorticity generated by swinging force tends to diffuse into the fluid interior and creates an average flow near the cavity walls that facilitates heat convection. With high-frequency swinging oscillations, the flow in the bulk of the closed cavity could consist of symmetrical vortical cells with the fluid moving along the cavity walls from their centers towards the corners, which forms the plan jets along the diagonals passing from the square corners to the duct core [11]. Depending on the combination of gravitational and vibrational Rayleigh numbers and pulsational Reynolds numbers, a variety of vortex-type average flows could develop in a swinging cavity. The interaction between the oscillation flow and buoyancy convection might result in the suppression of gravitational buoyancy effect. The consequent suppression of the resulting average flow accompanied by a reduction of the heat transfer, with the Nusselt number to be decreased by a factor of 2.7, has reported by Gershuni and Lyubimov [12]. Justified by the experimental evidences [10–12], it is likely that the rolling and pitching forces could considerably modify the flow pattern and heat transfer in a rib-roughened channel. Therefore the effect of pitching and/or rolling forces on heat transfer in a simulated cooling passage of shipping machinery must be fully understood if the confident design of heat transfer device for marine application is to be available.

This paper describes the results of a series of experiments aimed at studying the effects of rolling or/and pitching motions on heat transfer in a rectangular channel with two wider opposite walls roughened by 45° staggered ribs. The directions of swinging vectors for the rolling and pitching motions are both orthogonal to the mainstream direction in the rib-roughened channel. With the governing dimensionless flow parameters identified from the parametric analysis of the flow equations suitable of describing the thermal-fluids phenomena in a swinging duct [10], the parametric range of nominal sea-going conditions are specified and the flow conditions in a simulated cooling passage of plate type heat exchanger are accordingly reproduced and examined by the experimental apparatus. It is with the combined effects of surface ribs in a rectangular channel and the rolling and pitching motions that the present investigation is considered.

2. Strategy

The primary tasks of the present study are to investigate the heat transfer physics in a simulated cooling passage of plate-type heat exchanger under pitching and rolling environment and to acquire the heat transfer data for disclosing the combined effect of periodical 45° staggered ribs and swinging oscillations on heat transfer and generating the applicable correlations. As an attempt to study the thermal-fluid problems under the rolling and pitching environment, the general form of flow momentum equation with the swinging force-effects on fluid motion to be considered has been developed [10]. The modified version of Navier–Stokes equations that considers the effect of pitching and rolling forces on the fluid motion is usually convenient to describe the dynamic mechanism of the governing forces involved in a swing oscillation system. A study of the momentum and energy conservation equations, with the fluid motion referred to a coordinate system that swings with the flow boundary itself [10], suggests that the fluid motion and temperature field are, respectively, governed parametrically by the dimensionless equations (1) and (2).

$$\begin{aligned}(\mathrm{Ro}+\mathrm{Pi})\frac{\partial \widetilde{V}}{\partial \Gamma}+(\widetilde{V}\cdot\widetilde{\nabla})\widetilde{V}&=-\widetilde{\nabla}\widetilde{P}+\frac{1}{Re}\widetilde{\nabla}^2\widetilde{V}-2(\mathrm{Ro}\sin\Omega_{\mathrm{R}}t\vec{i}+\mathrm{Ro}\sin\Omega_{\mathrm{P}}t\vec{j})\vec{V}\\&+\left\{\frac{\mathrm{Bu}\eta\Omega_{\mathrm{P}}^2H_{\mathrm{P}}d}{W_{\mathrm{m}}^2}(\sin\Omega_{\mathrm{P}}t)^2\vec{i}+\frac{\mathrm{Bu}\eta\Omega_{\mathrm{R}}^2H_{\mathrm{R}}d}{W_{\mathrm{m}}^2}(\sin\Omega_{\mathrm{R}}t)^2\vec{j}\right\}\end{aligned} \tag{1}$$

$$\frac{\mathrm{D}\eta}{\mathrm{D}t}=\frac{1}{Re\,Pr}\widetilde{\nabla}^2\eta \tag{2}$$

where

$$Re=\frac{W_{\mathrm{m}}d}{\nu_0}\quad(\text{Reynolds number}) \tag{3}$$

$$\mathrm{Ro}=\frac{\Omega_{\mathrm{R}}d}{W_{\mathrm{m}}}\quad(\text{rolling number}) \tag{4}$$

$$\mathrm{Pi}=\frac{\Omega_{\mathrm{P}}d}{W_{\mathrm{m}}}\quad(\text{pitching number}) \tag{5}$$

$$\mathrm{Bu}=\beta_0\tau d\quad(\text{buoyancy parameter}) \tag{6}$$

$$\eta=\frac{(T-T_0)}{\tau d}\quad(\text{dimensionless fluid temperature}) \tag{7}$$

$$Pr=\frac{\mu_0C_{p_0}}{k}\quad(\text{fluid Prandtl number}) \tag{8}$$

All symbols in Eqs. (1)–(8) are referred and self-explained in the nomenclature section. The local coolant properties such as β_0, C_{p_0}, k_0, and μ_0, which were used to evaluate the controlling non-dimensional parameters such as Ro, Pi, Bu, and Re, were evaluated by means of standard polynomial functions with the reference flow inlet temperature T_0 as the determined variable. Note the gradient of duct-wise coolant bulk temperature rise, τ,

remains constant when the heat flux is uniformly distributed over the fluid-wall interface. The τ value varies with coolant mass flow rate and heat flux imposed. As the heaters used to heat the coolant experienced an external heat loss to the laboratory environment, the duct-wise heat flux was experimentally prescribed by subtracting the external heat loss from the total heat flux generated. The extent of this heat loss was assessed by means of a series of heat loss calibrations, which results could be well approximated as a linear function of the mean wall-to-ambient temperature difference at each swing frequency. Because of the linearity of the heat loss characteristic, it may be applied to local stream-wise positions when correcting the surface heat flux for external heat losses with flow. For any specific set of flow conditions tested, the duct-wise distribution of convective heat flux could be determined. Having determined the local enthalpy of flow, the coolant bulk temperatures were successively evaluated from the temperature measurement at the flow entrance, T_0, toward the exit plane of test duct. A linear regression routine with the intercept fixed at T_0 was followed to obtain the coolant bulk temperature gradient, τ. To verify this calculating process, the calculated exit flow bulk temperature and the measurement detected by thermocouple penetrating into the core of duct flow at the exit plane were constantly compared for each data batch generated. The data batch was collected when the differences between the calculated exit bulk temperatures and measurements were within $\pm 10\%$.

The non-dimensional parameters given by Eqs. (3)–(8) govern the heat transfer and fluid-flow in this swinging system. The Reynolds number, *Re*, may be interpreted as the ratio of fluid inertial forces to viscous forces in the usual manner. The rolling (Ro) and pitching (Pi) numbers have their origins from the Coriolis force components and express, respectively, the ratio of the rolling and pitching forces, induced by the swinging oscillation, to the fluid inertial force. The buoyancy parameter is treated as a ratio of temperature dependent fluid density perturbation to the fluid density at reference temperature, T_0. For a coolant with finite value of thermal expansion coefficient, β_0, this parameter only varies with τ. In the swinging rib-roughened channel where the flow could never steady, the buoyancy parameter could still couple with swinging acceleration in term of $\Omega_{R,P}^2 H_{R,P} \sin(\Omega_{R,P} t)\, i, j$ that yields to a different mode of buoyancy interaction from the typical gravity-type free convection. In the present unsteady flow system; it is unlikely to have the sufficient time for the development of **stable** buoyancy-driven body force differences over the cross plane of swinging duct. However the implementation of curl operation through Eq. (1) converts the momentum equation into an equation describing the vorticity transportation. The buoyancy term of $\nabla \times (\mathrm{Bu}\,\eta \Omega_{R,P}^2 H_{R,P} d \sin(\Omega_{R,P} t)\, i, j)$ remains as a source term to generate vorticity, which is a sign-varied temporal function. It is felt that the buoyancy interactions in the swinging duct are originated from their instant effects on the vorticity. The temporary varied vorticity field affected by the swinging buoyancy could lead to a dynamic mode of buoyancy interaction, which affects the fluid flow and heat transfer. The buoyancy parameter, Bu, at each combination of Ro, Pi and *Re* thus quantifies the relative degree of buoyancy interactions in this unsteady flow field, expresses the ratio of the buoyancy forces due to the effective body force field created by the swinging oscillation. When the streamwise fluid temperature gradient, τ, increases as a result of increasing convective heat flux for a given coolant's mass flow rate or decreasing the coolant mass flow rate at a given heat-flux value, the relative strength of buoyancy level enhances and the Bu value increases. This buoyancy parameter, Bu, could yield into other mathematical form of $\beta_0 \Delta T \frac{4}{Re\,Pr} \frac{d}{\Delta L}$ in which the temperature difference, ΔT, corresponds to the fluid temperature gradient normal to the heated wall over the length scale ΔL. This buoyancy parameter, Bu, treated as an index of relative strength of buoyancy level, provides convenience for engineering design applications. In a Grashof number, the temperature difference, which is customarily defined as the wall-to-fluid temperature difference, is convenient to be measured in the phase of research work, but is difficult to define in the design phase because the wall temperature remains unknown at the initial design stage. Therefore, the use of heat transfer correlation involving buoyancy effect requires several iterations in order to re-define the Grashof number and thus the Nusselt number in the design stage when the wall temperature distributions of a mechanical component are evaluated based on the presumed *Gr* values in the previous calculating process. For ducted flow, once the cooling duty, the coolant and the coolant flow rate are specified, the overall streamwise coolant temperature gradient could be readily defined as τ value. When the Nusselt number correlation is derived using the buoyancy parameter instead of the Grashof number, the downstream design process could be simplified. The Prandtl number, *Pr*, characterizes the fluid in the usual manner.

The solutions of Eqs. (1) and (2) are also subject to the hydrodynamic, thermal and geometric boundary conditions at the interface between the solid-wall and the coolant flow. These boundary conditions include the specific internal geometries of the ribs and duct selected. Because the range of variation in Prandtl number of coolant for the present study is less than 2.3%, the local Nusselt number, *Nu*, is parametrically link with Reynolds, pitching and rolling numbers and the buoyancy parameter, which may be expressed as

$$Nu = \Psi\{Re, \mathrm{Pi}, \mathrm{Ro}, \mathrm{Bu}, \text{boundary conditions}\} \tag{9}$$

where Ψ is an unknown function of *Re*, Pi, Ro and Bu and location in swinging channel. The local Nusselt number, *Nu*, is evaluated based on the temperature difference between heated wall and local flow bulk temperature, T_f, as

$$Nu = \frac{q_f d}{(T_w - T_f)k} \tag{10}$$

in which q_f is the convective heat flux to the fluid.

The parametric equation (9) forms the basis of the experimental strategy used for examining the effect of swinging oscillation on the cooling performance of the present flow geometry. By direct measurement of the duct-wise variation of Nusselt number with systematic changes in the controlling parameters of *Re*, Pi, Ro and Bu, their individual effects may be determined and isolated and the physics of heat transfer in association with the individual and combined effects of the non-dimensional groups appearing in Eq. (9) are unraveled. Note, in the limiting case of a condition having a vanishing small wall-to-fluid temperature difference but the test duct swings, the buoyancy interaction in Eq. (9) is vanished. However, for simulating of zero-buoyancy convective capability, which is impractical for heat transfer experiment owing to the fact that a real fluid has finite value of thermal expansion coefficient, the solution of heat transfer function Ψ in Eq. (9) was inferred by extrapolating a family of heat transfer data taken at a specific set of Reynolds, pitching and rolling numbers with different wall-to-fluid temperature differences to the scenarios of zero buoyancy. For a set of boundary conditions simulated by the present investigation, such as the geometrical features of rib-roughened surface, the sectional shape of test channel and the heating condition, the effects of the constituent dimensionless groups indicated in Eq. (9) are examined by systematically varying each of the flow parameters involved in Eq. (9). A subsequent data reduction program followed the definitions of the dimensionless groups shown in Eqs. (3)–(10), generates the non-dimensional raw data for further analysis.

3. Apparatus and program

3.1. Swinging facility

Fig. 1 shows the schematics of the rolling and pitching test facility used for the present investigation. An air receiver (1) was maintained at a pressure in the range of 6–8 bars by a compressor (2). The coolant, dehumidified air, from the receiver was cooled and allowed to flow through the rib-roughened channel (3), which simulates a cooling passage in the plate-type heat exchanger, via an air dryer (4), a combined pressure regulator and filter (5), a Tokyo Keiso TF-1120 mass flow meter (6), a needle valve (7) and a digitized pressure gauge (8). A flow calming section (9) of length equivalent to 15 duct hydraulic diameters was fitted immediately upstream of the abrupt entry plane of the heated test section. The area ratio of the entry plenum to the test channel was 15. It was noted that, as the oscillatory flow could develop in the swinging test duct (3), the mass flow meter (6) was allocated with a length of 200 hydraulic diameters upstream of the flow calming section (9). This mass flow measurement, which was used to define the nominal Reynolds number, was found steady even if the test channel (3) was swinging. The needle valve (7) was used to set the airflow through the test section at a level appropriate for the Reynolds number at which a particular experiment was to be conducted.

Two crank-wheel mechanisms (10), (11), each driven by a 1000 W DC electric motor via a reduction gearbox, were used to create the rolling and pitching motions of the test bed (12). The universal joints attached underneath the test bed converted the crank motion into vertical oscillation that facilitated the swinging motion of test bed. Speed fluctuations were minimized by means of the flywheels (13), (14). Also the counter balancing weight (15), (16) were adjusted and fitted to the flywheels in order to maintain dynamic balance. Two shafts (17), (18) that supported the rolling and pitching motions were separated. Therefore the rolling or pitching frequencies could be individually controlled. Two optical proximity transducers (19), (20) were used to measure the rotational speeds of the crank mechanisms and hence the swinging frequency and the angular velocity of the rolling and pitching motions. The heat transfer test module (21) was located at the corner of the test bed. The lengths of pitching and rolling arms are 1.2 and 0.6 m respectively that provides a length ratio of pitch arm to rolling arm of 2:1. This unequal rolling and pitching arms typifies a scenario that is commonly encountered by allocating a thermal-fluid device on a ship. Thus even if the frequencies of rolling and pitching motions are identical that simulates the harmonic compound oscillations; the rolling and pitching numbers are different.

3.2. Test section

Fig. 2 shows the constructional details of the heat transfer test module. Six skewed ribs with the attack angle of 45° were arranged in the staggered manner along each side of the two opposite heated walls. These two ribbed heating surfaces were made of a continuous 100 mm wide, 0.1 mm thick stainless steel foil (1). An electrical supply was connected to directly heat the ribbed stainless steel foils (1). A high-current, low-voltage DC electrical power supply was directly fed through the two opposite heating foils (1) to generate the uniform flux heating condition. Adjusting the heating power

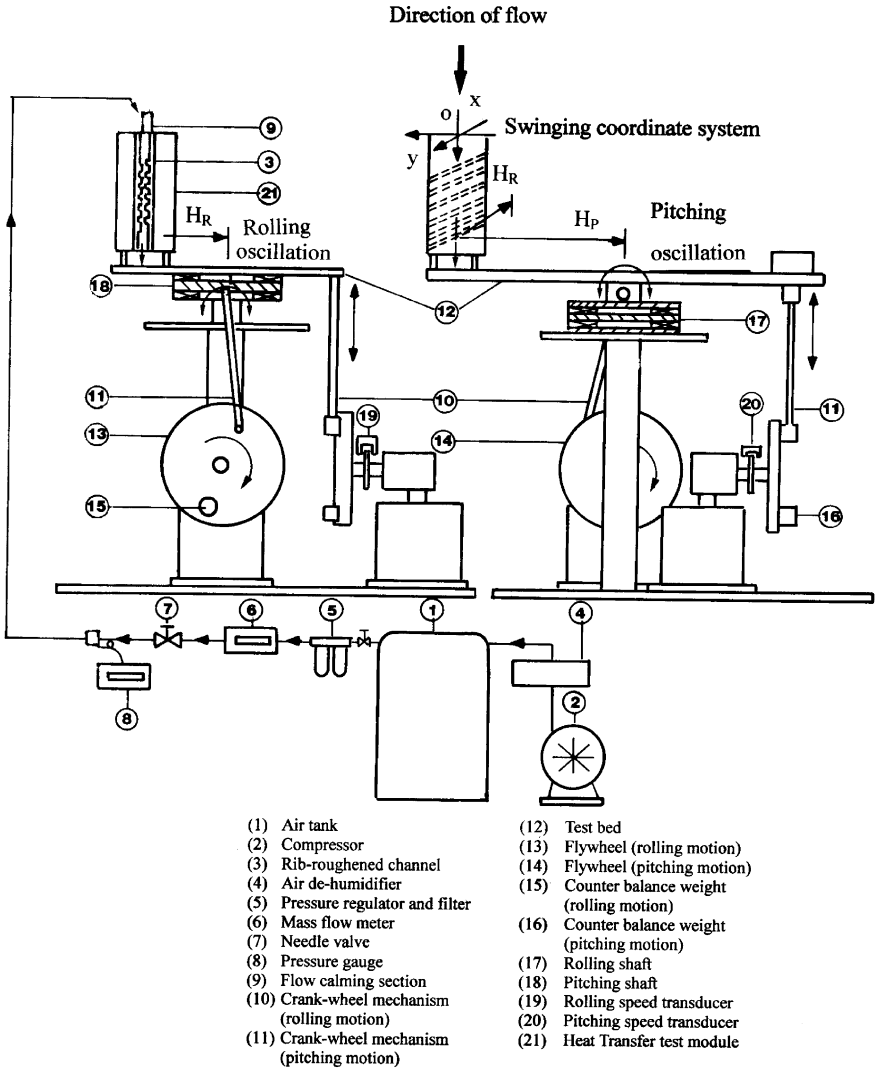

Fig. 1. Schematics of swinging test facility.

supply varied the relative strength of the buoyancy level at any fixed flow condition. Each ribbed heating foil (1) was clamped within four 20 mm thick Tufnol sidewalls (2) to secure its position in the test channel. Along the centerline of the rib-roughened surface, 10 K-type thermocouples were positioned on the back of the stainless steel heating foil (1) by sparkle welding to measure the wall temperatures at locations corresponding to the rib and mid-rib positions. Ceramic cement was filled in behind each rib after the wall thermocouples were positioned. The width and height of the rectangular test channel, encapsulated by four Tufnol sidewalls (2), were 100 and 15 mm respectively, which provided a 26 mm hydraulic diameter for the test channel. Geometric features of the rectangular test section were specified in terms of four non-dimensional groups defined in Fig. 2 as:

- rib attack angle $(\alpha) = 45°$ (Ribs on two opposite walls are offset by 0.5 pitch and angled in the same direction)
- channel width, $W(100\text{ mm})$/channel height, $H(15\text{ mm}) = 6.67$ (aspect ratio of test channel)
- rib height, $e(3\text{ mm})$/channel height, $H(15\text{ mm}) = 0.2$
- rib pitch, $P(30\text{ mm})$/rib height, $e(3\text{ mm}) = 10$
- rib land, $L(3\text{ mm})$/rib height, $e(3\text{ mm}) = 1$

Note the first and sixth ribs were, respectively, allocated at the immediate flow entrance and exit as indi-

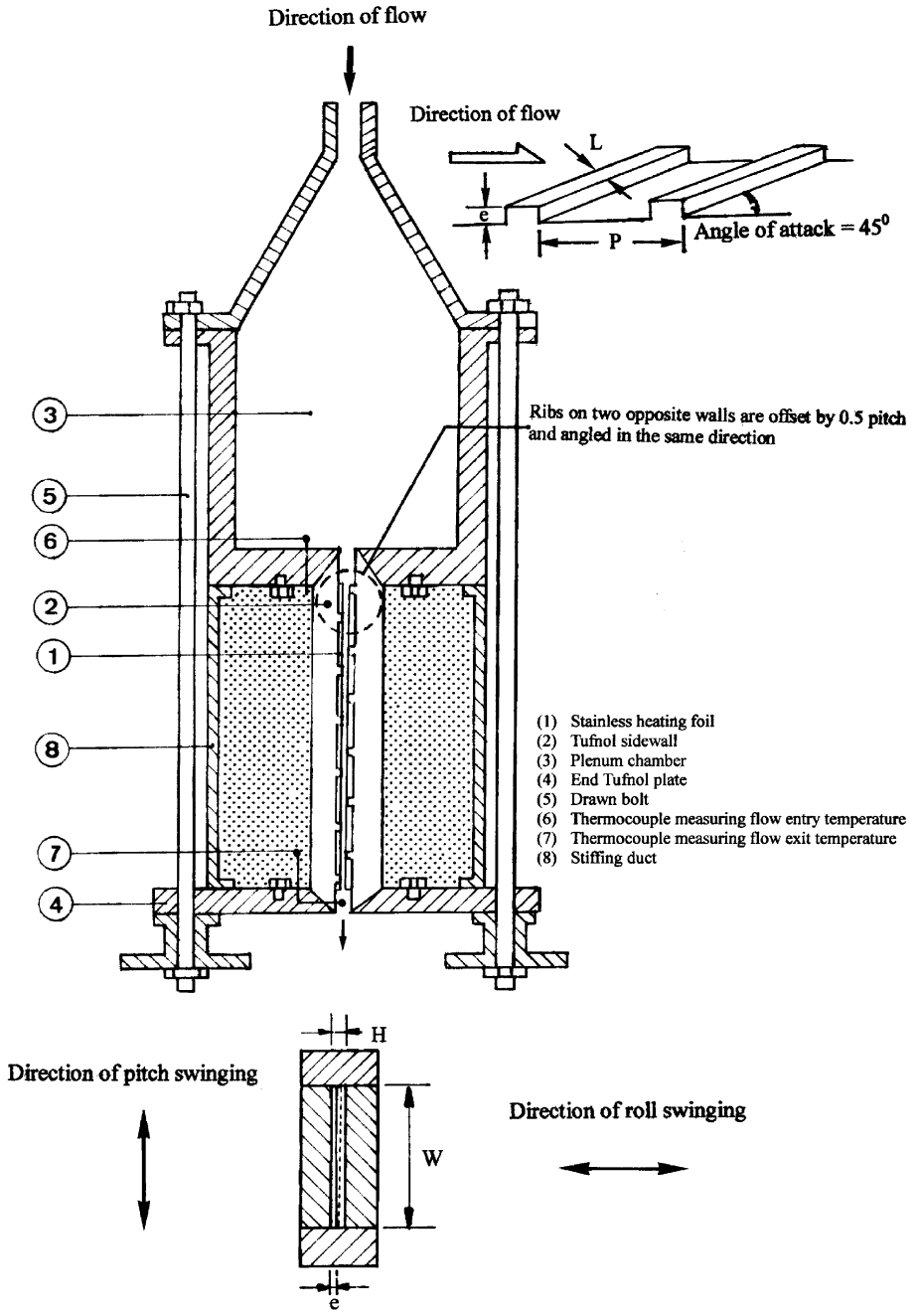

Fig. 2. Heat transfer test module.

cated in Fig. 2. The complete set of test section was tightened between the plenum chamber (3) and the end Tufnol plate (4) by four draw-bolts (5). A cubic plenum of width 150 mm (3) was consolidated with the test section to simulate the abrupt entry condition so that the re-developments of the thermal and hydraulic boundary layers initiated almost at the immediate flow entrance. The pressure and temperature of the entry air in this plenum chamber (3) were measured with a pressure transducer and a type K thermocouple (6) respectively. The inlet Reynolds number, for a particular set of experiment, could be calculated and monitored using the measured airflow, plenum chamber pressure and flow entry temperature. This inlet Reynolds number was

based on the hydraulic diameter of the test section. At the exit plane of the rectangular coolant passage, three type K thermocouples (7) penetrated into the core of test channel at three different spanwise locations. The flow bulk temperature at the exit plane of test channel was obtained by averaging these three temperature measurements detected from the thermocouples (7). Note, no thermocouple allocated within the flow path as indicating in Fig. 2 in order to avoid the upstream and downstream disturbances induced by penetrating thermocouples into flow passage. A convergent cubic chamber with 30° of convergence connected the plenum chamber (3) with the coolant supply system. The in fill of thermal insulation material packed in the space between the test section and the stiffening duct (8) in order to minimize external heat loss. For the test performing at the highest temperature level and swinging frequencies, the estimated heat loss during the experiment was about 11.8% of the total heater power supply. The built up heat transfer test module was vertically mounted onto the swinging facility so that the vectors of rolling and pitching oscillations were both orthogonal to the main flow direction. The wide and narrow sides of the test channel were, respectively, coincided with the directions of pitching and rolling motions. All the temperature measurements were monitored and stored in a IBM PC using a Net-Daq Fluke Hydra 2640A data logger for the subsequent data processing.

3.3. Program

This experimental program has three phases:

1. Initially the heat transfer performance of the static channel was investigated to study the effect of Reynolds number on the heat transfer over the rib-roughened surface. The heat transfer correlation generated in this phase was treated as the static reference to compare against the swinging heat transfer data generated in the second phase and as the heat transfer solution of zero swinging oscillation for the data analysis in the third phase.

2. The second phase involved a systematic investigation of the combined effect of swinging buoyancy together with the system oscillations under single and compound modes of swinging motions. The range of experimental parameters covered was typical of those encountered for the sea-going practice of a merchandized ship.

3. The third phase involved an attempt to generate empirical heat transfer correlations to permit all the relevant physical effects governing the system's behavior to be examined. The interactive effect of forced convective inertial force, buoyancy and the effective body forces induced by the rolling or/and pitching motions has been unraveled.

Note the swinging heat transfer data was produced at a value of fixed Reynolds numbers. At each selected Reynolds number, tests at swinging frequencies of 0.333, 0.667 and 1.0 Hz, which frequencies were used individually by three different swinging conditions, namely the rolling, pitching and compounds rolling and pitching oscillations, were performed. For the tests involved simultaneous rolling and pitching oscillations, both harmonic and non-harmonic swinging conditions were examined. The non-harmonic swinging oscillations were created when the rolling and pitching frequencies were not equal. When each compound rolling and pitching test is performed, the driven cranks for both pitching and rolling motions are re-set to their top dead points so that the peaks of rolling and pitching motions are in phase when the frequencies of rolling and pitching motion remain identical. However, for the non-harmonic test, the rolling and pitching motions are out of phase in a periodical manner even if the initially starting phase angles for rolling and rolling motions are the same. At each predefined Reynolds, rolling and pitching numbers, five different levels of heater power were used to permit an assessment of the effect of buoyancy on heat transfer. Actual heater powers were selected to create a test section nominal wall temperature of 60°, 80°, 100°, 120° and 150 °C at the sixth rib location. For each individual test, the apparatus was allowed approximately 45 min to achieve the thermal equilibrium state. A thermal equilibrium state was assumed when the variations of the time-averaged wall temperatures remained within ± 0.3 °C. The on-line data acquisition and storage system was then activated and captured all relevant measurements for a total scan period of 20 s. In this respect, the time response for the measurement system was adjusted to 0.05 s/scan. This measurement rate was capable of resolving changes on the time-averaged scale for swinging tests at a maximum frequency of 1.0 Hz. However, this measurement rate might be insufficient to detect the full time-varied temperature variations for a swinging cycle. Therefore the temporally varied temperature levels over the 20-s 'equilibrium state' were automatically logged and averaged. These measurements were used to define the time-averaged Nusselt number data for a particular experiment. The raw experimental data was subsequently processed to generate the appropriate Reynolds number, the rolling and pitching numbers and the buoyancy parameter; and the individual effect of these parameters on the Nusselt number distribution examined. The range of these non-dimensional parameters is given in Table 1.

An uncertainty approximation for the data reduction was conducted [13]. As the properties of the coolant were estimated from the flow bulk temperature, the major source of uncertainty for evaluating the non-dimensional parameters was attributed from the temperature measurement. As the thermal equilibrium state

Table 1
Range of experimental non-dimensional parameters

Non-dimensional parameter	Range
Reynolds number	2100–12000
Rolling number	0–0.0058
Pitching number	0–0.003
Buoyancy parameter	0.0016–0.0083

was assumed when the variations in local temperature were in the range of ±0.3 °C, the maximum uncertainty in temperature measurement was estimated as ±0.3 °C. With the wall-to-fluid temperature differences varied from 28 to 87 °C, the maximum uncertainty for *Nu*, *Re*, Ro, Pi and Bu were about 15%, 6.8%, 1.8% 1.5%, and 4.1% respectively.

4. Results and discussion

4.1. Static channel

In the absence of swinging oscillation, Eq. (8) shows that the local heat transfer in the static channel is reduced to a function of *Re* and Bu for a predefined set of boundary conditions. Fig. 3 depicts the streamwise heat transfer variations in the static channel at Reynolds numbers of 3000, 6000 and 9000 with five different heater powers for each Reynolds number tested. As seen in Fig. 3, the results obtained with five different heater powers at each Reynolds number collapse into a tight data band at each axial location that indicates the negligible buoyancy effect in the static channel. The apparent streamwise zigzag heat transfer variation along the rib-roughened surface is detected by the present arrangement of wall-temperature thermocouples, which pattern is attributed to the agitated flow field created by the penetrating ribs. The Nusselt numbers at the rib locations are consistently lower than their downstream counterparts at the mid-rib locations. The heat transfer difference between the rib and its successive mid-rib locations is in the order of 35–50% of the heat transfer level at the rib location. Thus the present ribbing geometry that involves the 0.2 channel height of rib-penetration on each wide side of test channel has provided considerable effects on the flow and heat transfer inside the rectangular channel. Also compared in Fig. 3 are the heat-transfer measurements generated by Han et al. [1] at Reynolds number of 8761. The geometrical conditions tested by Han et al. [1] are similar with the present rib surface but the rib-height to channel-height ratio examined by Han et al. [1] was 0.622 that is about 1/3 of the present rib penetration. As shown, the Nusselt numbers reported by Han et al. [1] generally agree with the present results while the less amount of streamwise data oscillations are observed in the data trend of Han et al. [1] due to the relatively shallow rib penetration.

On moving downstream from the entry toward the exit plane, the zigzag heat transfer variations are accompanied with a weak tendency of heat transfer decay from the immediate entry region towards a "periodic repeated" range. This gradual axial heat transfer decay that approaches the developed "periodic repeated" range is caused by the abrupt entrance effect and is consistent with the development of the "periodically disturbed" boundary layer [2]. With the surface ribs present the Nusselt number achieves a more or less "repeated rib" region after of four ribs. Fig. 3 also compares the static Nusselt number, Nu_0, to the Dittus–Boelter correlation level [14], Nu_∞, demonstrating the heat transfer augmentation provided by these surface

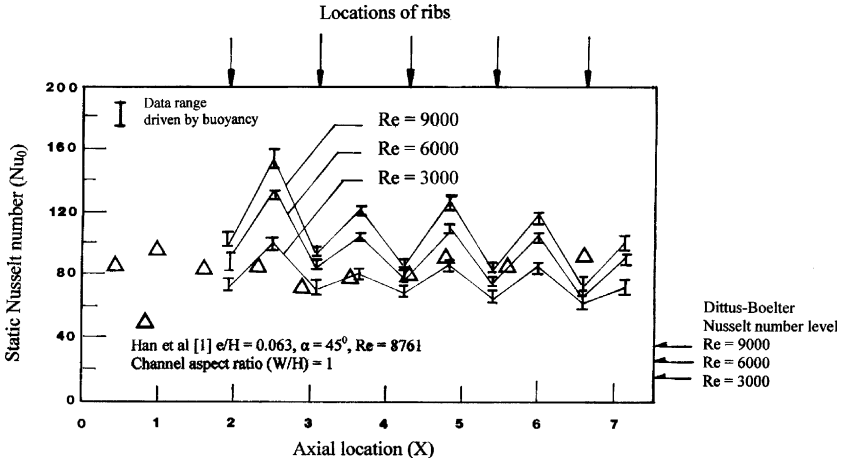

Fig. 3. Streamwise heat transfer variations in static channel at Reynolds numbers of 3000, 6000, and 9000.

ribs. The heat transfer augmentation in the range of 3–5.6 times of the Dittus–Boelter level [14] appears to be axial-location dependent due to the rib associated flow phenomena and the developing nature of flow in the entry region. As the buoyancy effect on heat transfer in the static channel is ineffective, the heat transfer correlation may thus be developed individually at each rib and mid-rib locations, by an equation of:

$$Nu_0 = A(X) \times Re^{B(X)} \tag{11}$$

where A and B are correlated coefficients varying with axial location. Table 2 shows the numerically correlated coefficients A and B at the rib and mid-rib locations. Of the entire range of static Nusselt number data 95% are found to agree within $\pm 15\%$ of the correlation. Note in Table 2, the exponents of Reynolds number, B, decrease when the rib or mid-rib number increases. The level of exponent, B, mathematically indicates the dependency of Nusselt number on Reynolds number, which physically reflects the effectiveness of forced convective inertia on static heat transfer. The downstream decay of exponent, B, with a tendency to reach the asymptotic values of 0.195 and 0.3 at the rib and mid-rib locations, respectively, shown in Table 2 suggests that the influences of forced convective inertia on heat transfer are gradually weakened when flow approaches the repeated rib region from the abrupt entrance. Justified by this asymptotical variation manner, the flow reaches the repeated rib flow region after traverses four pairs of ribs where the flow and heat transfer characteristics become periodically repeated. Accompanying with the decay of B exponent along the static channel is the corresponding increase in coefficient A, which could be treated as an indication of the heat transfer enhancement attributed by the rib-induced cross-plane swirling flow and the rib-modified flow structures.

Eq. (11) correlates the entire range of static Nusselt number data, which is treated as the reference to normalize the swinging heat transfer results in order to reveal the effects of swinging oscillations on heat transfer in the rib-roughened rectangular channel.

Table 2
Coefficients A and B at measured axial locations

X location	Coefficient A	Coefficient B	Rib/mid-rib location
1.98	5.835	0.3141	Rib 1
2.56	3.751	0.4094	Mid-rib 1
3.13	9.511	0.2515	Rib 2
3.71	3.593	0.3883	Mid-rib 2
4.29	14.516	0.1995	Rib 3
4.87	4.885	0.3581	Mid-rib 3
5.44	14.899	0.1867	Rib 4
6.02	7.458	0.3016	Mid-rib 4
6.6	14.986	0.1952	Rib 5
7.17	7.105	0.3007	Mid-rib 5

4.2. Swinging channel

The general heat transfer effect of single rolling and pitching oscillations and the compound rolling and pitching oscillations with harmonic and non-harmonic rhythms is illustrated based on a particular set of experiments performing with various swinging frequencies at a fixed Reynolds number. Fig. 4 shows the swinging heat transfer results obtained at Reynolds number of 7000. The heat transfer data depicted in Fig. 4(a) and (b) is generated with single mode of swinging oscillation. The rolling and pitching numbers in Fig. 4(a) and (b) are both controlled at 0.001. Note, due to the different lengths of swinging arms for pitching and rolling oscillations, the pitching and rolling frequencies are 0.667 and 0.333 Hz respectively. Fig. 4(c) and (d) illustrate the heat transfer results affected by the compound rolling and pitching oscillations with harmonic and non-harmonic rhythms. The harmonic rhythm of rolling and pitching oscillations is controlled at frequency of 0.667 Hz, which produces the pitching and rolling numbers of 0.001 and 0.002 as indicated in Fig. 4(c). The pitching and rolling frequencies selected to create the non-harmonic oscillations are 0.667 and 1 Hz that generates the pitching and rolling numbers of 0.001 and 0.0031 respectively. The Nusselt number reference in the static channel is plotted as the solid line in each plot of Fig. 4, against which the swinging data is compared to assess the effects of swing oscillations on heat transfer.

The streamwise heat transfer variations found in the swinging channel as shown in Fig. 4 follow the general pattern observed in the static channel in which the heat transfers gradually decay toward a developed level accompanying with the agitated saw-tooth variations. Although the most of heat transfer data generated at Reynolds number of 7000 shown in Fig. 4 is improved from the static-channel level, the heat transfer impediments relative to the static reference are found with the single pitching oscillation and with the non-harmonically compound pitching and rolling oscillations. The streamwise saw-tooth heat transfer variations are still evident in the swinging channel with all the conditions tested, which indicates the dominant rib effect on heat transfer even if the swinging forces prevail over the rib-roughened channel. The test results depicted in Fig. 4(a) and (b) are obtained with the same value of pitching and rolling numbers of 0.001, which fixes the relative strengths of rolling and pitching forces to the convective inertia at Reynolds number of 7000. The larger amounts of heat transfer difference between the swinging and static results are found for rolling oscillation when the

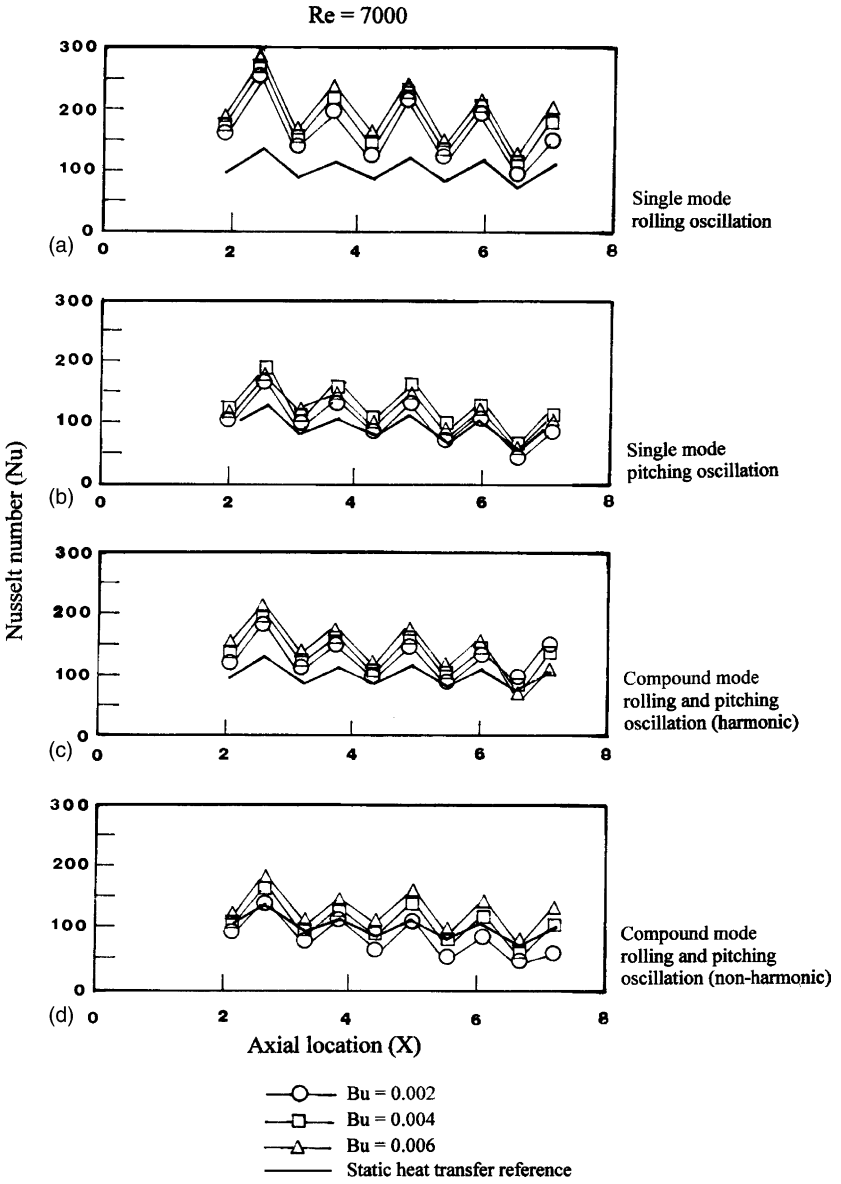

Fig. 4. Streamwise heat transfer distributions in swinging channel at Reynolds number of 7000. (a) Ro = 0.001, Pi = 0, f_R = 0.33 Hz. (b) Ro = 0, Pi = 0.001, f_P = 0.667 Hz. (c) Ro = 0.002, Pi = 0.001, f_R = 0.667 Hz, f_P = 0.667 Hz. (d) Ro = 0.0031, Pi = 0.001, f_R = 1 Hz, f_P = 0.667 Hz.

results depicted in Fig. 4(a) and (b) are compared. This different degree of swinging effect on heat transfer between the single rolling and pitching oscillations justifies the greater swinging force effect across the narrow side of a rectangular channel. The heat transfer performances generated with harmonically and non-harmonically compound oscillations as revealed in Fig. 4(c) and (d) are worse than that affected by the single rolling oscillation at the rolling number of 0.001. It is unlikely that the effect of compound rolling and pitching oscillations on heat transfer is the addition of two individual single-mode oscillating effects but appears to be the complex synergetic influence. The importance of buoyancy in the swinging rib roughened channel is indicated in Fig. 4 as the data spreads driven by varying the buoyancy level at each axial station measured. In this respect, the buoyancy effect could either improve or impede local heat transfer, which effect is dependent on the axial location, the values of rolling and pitching numbers and the mode of swinging oscillation. The

general swinging force effects on heat transfer in the present test channel unraveled by Fig. 4 are considerable and consistent with all the oscillating experiments undertaken.

Due to the development of periodically repeated rib flows after the coolant traverses about four pairs of ribs, the streamwise heat transfer distributions in the developed periodical region repeat so that the heat transfer correlations developed at locations of rib 5 and mid-rib 5 feature the heat transfer performances in the repeated flow region. Nevertheless, in the attempt to demonstrate that the experimental strategy developed by the present study with the aim of deriving the heat transfer correlation is also applicable in the developing flow region, the demonstration of generating correlative type of Nusselt number equations is illustrated using the data measured along the entire rib-roughened surface. However, only the correlations developed for the rib 5 and mid-rib 5 locations, those feature the heat transfer performances in the repeated flow region, are presented. To derive the correlating equation that permits the individual and synergic effects of inertial, swinging and buoyancy forces on heat transfer to be evaluated, the isolation of *Re* variable from Eq. (9) could considerably simplify this strategic task. In the static channel, Eq. (11) has unraveled the physical impacts of *Re* variable on heat transfer. Following the assumption that the *Re* effect on heat transfer could be uncoupled from the swinging force effects, the normalizing Nusselt number in terms of Nu/Nu_0 shall be independent of Reynolds number. Also the ratio of Nu/Nu_0 could directly indicate the effect of swinging mechanism on heat transfer. To examine the isolation of *Re* variable from the swinging force effects, three sets of illustrative examples are depicted in Fig. 5, where the streamwise distributions of normalized Nusselt number, Nu/Nu_0, are produced from three different Reynolds numbers but at the fixed rolling or pitching numbers with the similar value of buoyancy parameter. As seen in Fig. 5(a) and (b), the range of data spread caused by varying Reynolds number from 2100 to 7000 is less than 10%. These plots also show the tendencies of improved data convergence and of decreasing Nu/Nu_0 value in the further downstream. The data-collapsing tendency demonstrated in Fig. 5 suggests that the *Re* variable effect on heat transfer in a swinging channel could be well quantified by $Re^{B(Z)}$ relationship and uncoupled from the swinging force effects. As the physical impacts of Reynolds number could be uncoupled from the swinging force effects, the individual effect of rolling and pitching forces on heat transfer without buoyancy interaction is now attainable.

The so-called "zero-buoyancy" swinging heat transfer data is inferred by extrapolating a series of swinging heat transfer data in terms of Nu/Nu_0 generated with different buoyancy levels at fixed flow and swinging

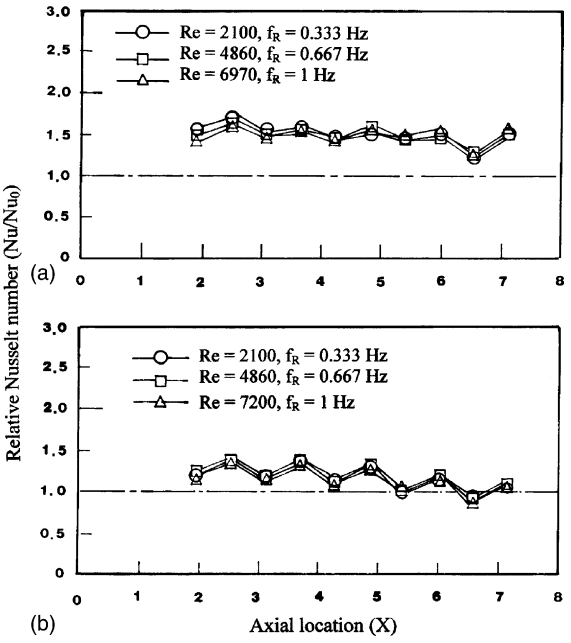

Fig. 5. Axial distributions of normalized Nusselt number with single-mode swinging oscillations at rolling number of 0.0025 and pitching number of 0.0028. (a) Ro = 0.0025, Bu = 0.0073, Pi = 0. (b) Pi = 0.0028, Bu = 0.0068, Ro = 0.

situations back to the condition of Bu = 0. Fig. 6 shows an illustrative example of generating the zero-buoyancy asymptotic heat transfer data for single and compound swinging oscillations. At the fifth rib location, the normalized Nusselt numbers obtained with five ascending buoyancy parameters for each selected Ro–Pi combination are numerically extrapolated back to the origin that reveal the zero-buoyancy heat transfer level. Following the data trend depicted in Fig. 6, which is a common trend for all sets of swinging test results, a liner correlating equation is adopted. The intercept of each linear correlating line depicted in Fig. 6 is collected as the zero-buoyancy heat transfer solution, which is a function of rolling and pitching numbers, the mode of swinging oscillation; and varies with the axial location. The positive and negative slopes of correlating lines shown in Fig. 6 respectively reflect the improving and impeding heat transfer effects due to the buoyancy interaction. In this regard shown in Fig. 6(c) and (d), the slope of each correlating line varying from positive to negative values demonstrates the reversal buoyancy effect from improving to impeding heat transfer. The increase of rolling or pitching numbers for the single mode swinging oscillation, as shown in Fig. 6(a) and (b), respectively reduces and increases the values of Nu/Nu_0. Led by the detailed examination of all axial location versions of Fig. 6, it is proposed that the specific form of

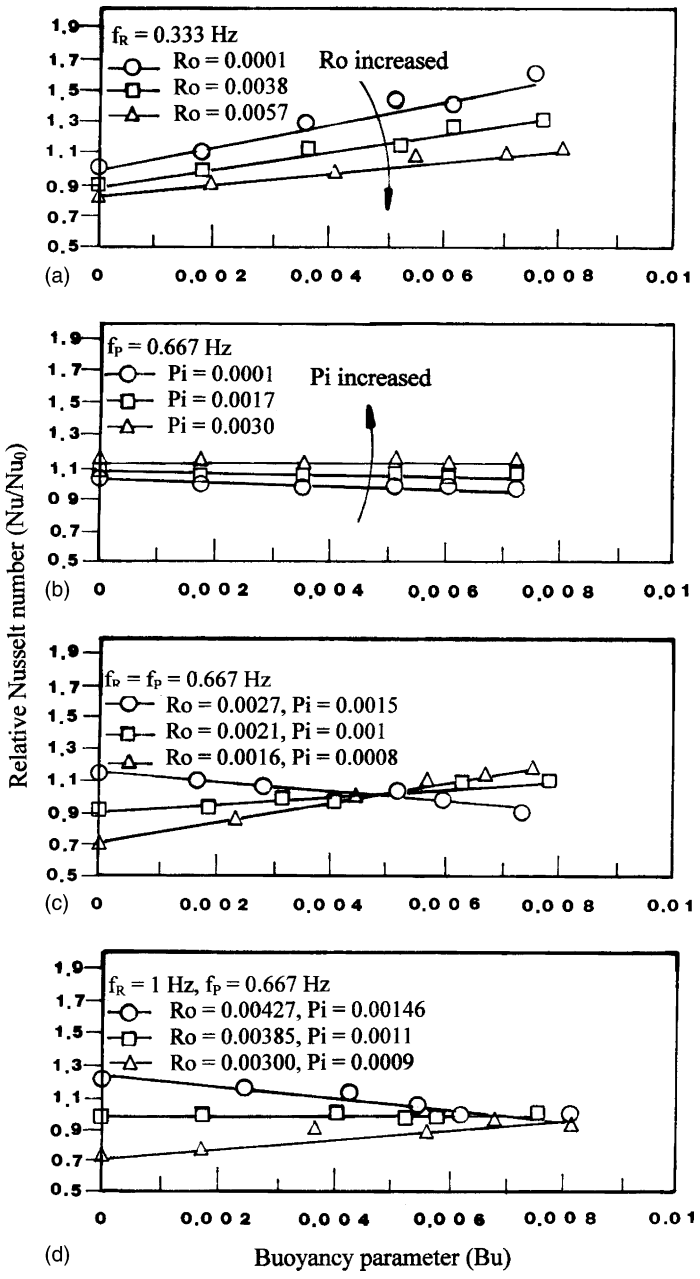

Fig. 6. Heat transfer variation with buoyancy parameter in swinging channel at fifth rib location. Single mode (a) rolling and (b) pitching oscillation. Compound mode rolling and pitching oscillation with (c) harmonic and (d) non-harmonic rhythm.

heat transfer correlation for single-mode swinging oscillation could be

$$\left.\frac{Nu}{Nu_0}\right|_{\text{Single-mode swinging oscillation}} = \Phi_{R,P}(\text{Ro or Pi}, X) + \varphi_{R,P}(\text{Ro or Pi}, X) \times \text{Bu} \quad (12)$$

where $\Phi_{R,P}$ and $\varphi_{R,P}$ are functions of rolling number, pitching number and axial location. The values of $\Phi_{R,P}$ and $\varphi_{R,P}$ are respectively collected from the intercept and the slope of each correlating line typified in Fig. 6. The variations of extrapolated zero-buoyancy heat transfer data, $\Phi_{R,P}$, with rolling or pitching number at rib and mid-rib locations under the single-mode swinging

conditions are separately grouped in Fig. 7(a–d). As seen in the plots of Fig. 7, the zero buoyancy heat transfer data tends to vary linearly with rolling or pitching number. There is axial location sensitivity of $\Phi_{R,P}$ on the number of rib and mid-rib traversed by flow as seen Fig. 7. A physical constraint that requires $\Phi_{R,P}$ remaining unity at zero values of rolling and pitching numbers reassembles the static heat transfer results correlated by Eq. (11). It is thus proposed that the relative heat transfer without buoyancy interaction under the single-mode swinging condition can be reasonably well approximated by an equation of the following general form

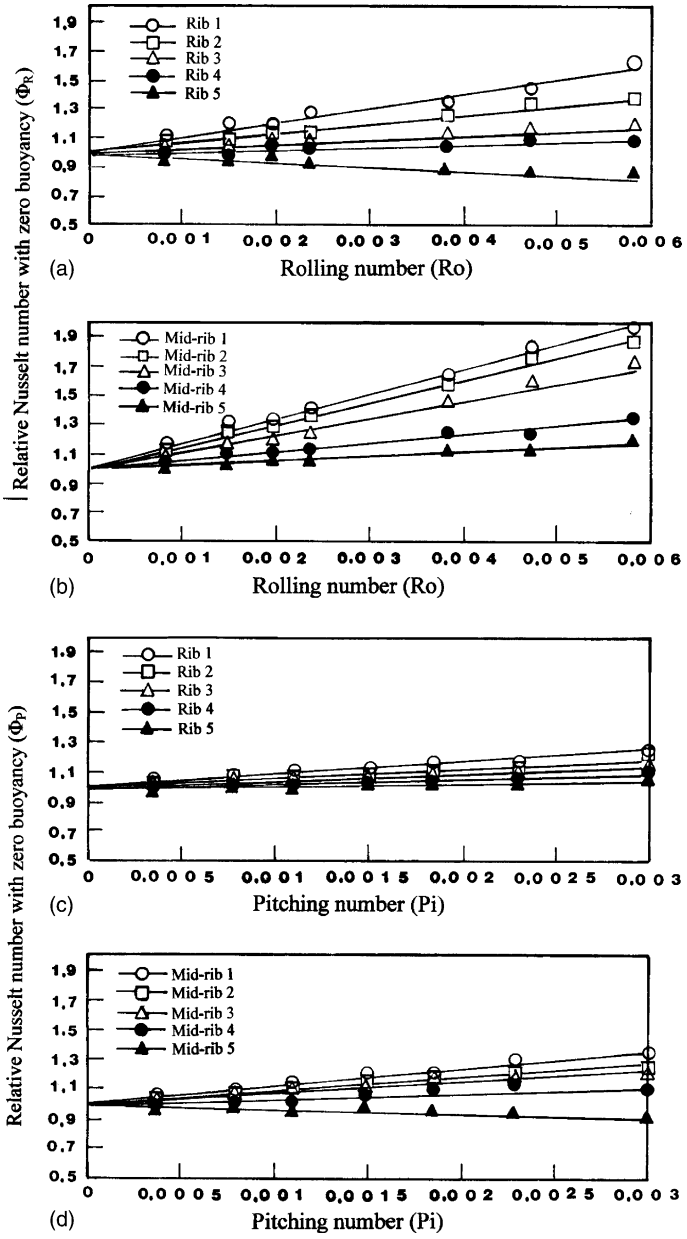

Fig. 7. Variations of extrapolating zero-buoyancy heat transfer with rolling or pitching number for single mode swinging oscillation. Single mode (a) rolling (rib locations), (b) rolling (mid-rib locations), (c) pitching (rib locations) and (d) pitching (mid-rib locations) oscillation.

$$\left.\frac{Nu}{Nu_0}\right|_{\mathrm{Bu}=0}^{\text{Single rolling}} = \Phi_{\mathrm{R}} = 1 + \psi_{\mathrm{R}}(X) \times \mathrm{Ro}$$

$$0 \leqslant \mathrm{Ro} \leqslant 0.0058 \tag{13}$$

$$\left.\frac{Nu}{Nu_0}\right|_{\mathrm{Bu}=0}^{\text{Single pitching}} = \Phi_{\mathrm{P}} = 1 + \psi_{\mathrm{P}}(X) \times \mathrm{Pi}$$

$$0 \leqslant \mathrm{Pi} \leqslant 0.003 \tag{14}$$

where ψ_{R} and ψ_{P} are the slopes of the correlating lines depicted in Fig. 7 that vary with axial location. As seen in each plots of Fig. 7, the values of ψ_{R} and ψ_{P}, systematically reduce in the further downstream. At the mid-rib locations for rolling oscillation (see Fig. 7(b)) and at the rib location for pitching oscillation (see Fig. 7(c)), the swinging force effects improve heat transfer in the present parametric ranges tested. In Fig. 7(a) and (d), the slopes of correlating lines gradually decrease and turn into negative values at the fifth rib and mid-rib locations. The relative heat transfer data collected at the rib locations for rolling oscillation (see Fig. 7(a)) and at the mid-rib locations for pitching oscillation (see Fig. 7(d)) initially shows continuous improvement from the stationary level when Ro or Pi increases up to about the fifth rib and mid-rib locations. At the fifth rib and mid-rib locations shown in Fig. 7(a) and (d) respectively, heat transfer is continuously reduced from the static references when the swinging force increases. Note that the results obtained with single rolling oscillation generally show the larger ψ values than the pitching counterparts, which result reconfirms the greater swinging force effect across the narrow side of a rectangular channel.

The manner of $\varphi_{\mathrm{R,P}}$ function varying with swinging number (Ro, Pi) at the fifth rib and mid-rib locations is shown in Fig. 8 to demonstrate the buoyancy effect on heat transfer. The results typified in Fig. 8(a) for single rolling oscillation show the consistent reduction in φ_{R} value when Ro increases. In the present range of rolling number tested, the φ_{R} function always remains positive at these two axial locations, indicating the improving heat transfer due to buoyancy interaction. With single pitching oscillation that directs the swinging force across the wide side of rectangular channel, the data points collected in Fig. 8(b) show the generally increasing tendency when pitching number increases. The values of φ_{P} increase from negative to positive values when pitching number increases. The cross-over condition, at which the φ_{P} function varying from negative to positive value, spots at the pitching number about 0.0025. The cross-over condition demonstrates the reversal buoyancy effect on heat transfer from the initial impediment to improvement when the pitching number increases to about 0.0025. The swinging forces directed across the narrow and wide sides of the test channel interact with buoyancy differently which leads to various data trends revealed in Fig. 8(a) and (b). Although the buoyancy interaction in the present swinging channel is complex, the detailed examination of all axial location versions of Fig. 8 permits a specific form of correlation for $\varphi_{\mathrm{R,P}}$ function that could capture the reversal buoyancy effect as:

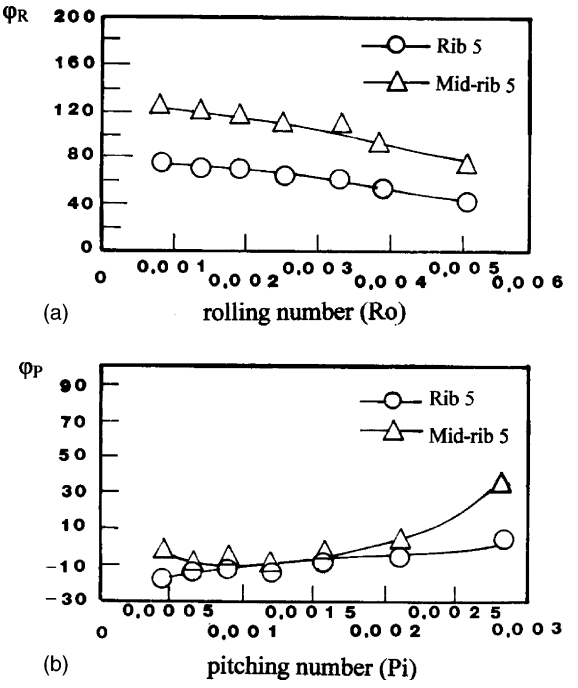

Fig. 8. Variations of $\varphi_{\mathrm{R,P}}$ functions with rolling or pitching number at rib 5 and mid-rib 5 locations. Single mode (a) rolling and (b) pitching oscillation.

$$\varphi_{\mathrm{R,P}}|_{\text{Single–mode swinging oscillation}} = C_1(X) + C_2(X) \times (\mathrm{Ro} \text{ or } \mathrm{Pi}) + C_3(X) \times (\mathrm{Ro} \text{ or } \mathrm{Pi})^2$$

$$0 \leqslant \mathrm{Ro} \leqslant 0.0058, 0 \leqslant \mathrm{Pi} \leqslant 0.003 \tag{15}$$

where C_{s} functions are the correlating coefficients for each data trend typified in Fig. 8 that vary with axial location. Tables 3 and 4 respectively list the numerically determined curve fits for $\psi_{\mathrm{R,P}}$ and C_{s} functions at the rib 5 and mid-rib 5 locations.

The heat transfer correlation that complies with the physical considerations under the single-mode rolling or pitching environment has been derived as Eq. (16) with the general form of

$$\frac{Nu}{Nu_0} = \Re(\mathrm{Ro}, \mathrm{Bu}, X) \text{ single rolling oscillation}$$
$$= \wp(\mathrm{Pi}, \mathrm{Bu}, X) \text{ single pitching oscillation} \tag{16}$$

The functions $\Re$ and $\wp$ in Eq. (16) quantify the heat transfer modifications produced by the single rolling or pitching oscillation, respectively. The heat transfer in the

Table 3
$\psi_{R,P}$ functional values for single swinging oscillation at rib 5 and mid-rib 5 locations

X location	ψ_R	ψ_P	Repeated flow region
6.6	−31.349	23.31	Rib 5
7.17	30.984	−28.73	Mid-rib 5

rib-roughened channel as affected by the combined rolling and pitching oscillations is not the additive results of the functions $\Re$ and $\wp$, as illustrated previously in Figs. 4 and 6. The parameters selected in the general correlating function to account for the synergistic effect of compound rolling and pitching oscillations shall reduce to a zero value when either the rolling or pitching oscillations vanish. With this consideration, the convenient parameters that account for the synergistic effects of the rolling and pitching oscillations are assumed as Ro × Pi and Ro × Pi × Bu, respectively, to correlate the heat transfer data affected by the compound swinging oscillation with and without buoyancy interaction. A general heat transfer equation that accounts for the individual and synergistic effects of the rolling and pitching oscillations with and without buoyancy interaction is assumed as:

$$\frac{Nu}{Nu_0} = \Re(\mathrm{Ro},\mathrm{Bu},X) + \wp(\mathrm{Pi},\mathrm{Bu},X) + \xi(\mathrm{Ro}\times\mathrm{Pi},X) + \zeta(\mathrm{Ro}\times\mathrm{Pi}\times\mathrm{Bu},X) \quad (17)$$

The experimental data of ξ function in Eq. (17) is obtained by subtracting the $\Re$ and $\wp$ functional values from the extrapolating $\frac{Nu}{Nu_0}$ data inferred by the procedure illustrated in Fig. 6(c) and (d) for approximating the zero-buoyancy heat transfer level under compound rolling and pitching environment. Because the compound-mode swinging heat transfer data at a specific buoyancy level is generated by experiment, the ζ function is evaluated using Eq. (17) once the values of $\Re$, $\wp$ and ξ are determined. In order to recast the heat transfer solution with single-mode swinging oscillation, the additive value of ξ and ζ functions has to be −1 when either the rolling or pitching numbers reduce to zero. The zero-buoyancy heat transfer solution with compound rolling and pitching swinging oscillation requires zero value of ζ function when Ro × Pi × Bu approaches zero. These two physical constraints for the ξ and ζ functions are well reflected in the data trends typified in Fig. 9(a) and (b), where the variations of ξ and ζ functions against Ro × Pi and Ro × Pi × Bu at locations of rib 5 and mid-rib 5 are examined. The data trends in all the axial versions of Fig. 9(a) are converged toward −1 when Ro × Pi approaches zero. Also the data points, typified in Fig. 9(b), converge toward zero when the parameter Ro × Pi × Bu becomes zero. The zero-buoyancy synergistic effects with harmonic and non-harmonic swinging oscillations, as demonstrated in Fig. 9(a), exhibit an initial heat transfer reduction, which is followed by a tendency of heat transfer recovery when the value of Ro × Pi increases. The values of ζ function consistently decrease with the increased value of Ro × Pi × Bu as shown in Fig. 9(b). Using a series of cross plots, based on Fig. 9 but applied to all axial locations, a series of curves may be interpolated, which correlated the values of ξ and ζ at each specified location. the variation of ξ and ζ values described as the functions of Ro × Pi and Ro × Pi × Bu respectively could be well correlated by the following equations of

$$\xi = -1 + F_1(X)\times(\mathrm{Ro}\times\mathrm{Pi}) + F_2(X)\times(\mathrm{Ro}\times\mathrm{Pi})^2 \quad (18)$$

$$\zeta = G(X)\times(\mathrm{Ro}\times\mathrm{Pi}\times\mathrm{Bu}) \quad (19)$$

where the F_s and G functions are the numerically determined curve-fitting coefficients. The curves in Fig. 9(a) and (b) represent the correlative results of Eqs. (18) and (19). Tables 5 and 6 respectively summarize the correlated values of F_s and G functions at the rib 5 and mid-rib 5 locations.

The overall success of the correlation result is indicated in Fig. 10, where all the experimental data are compared with the correlative prediction provided by Eq. (17). As revealed in Fig. 10, the swinging force effect complicated by the buoyancy interaction could cause heat transfer varying in the range of 0.75–2.5 times of the static channel value. The maximum discrepancy of

Table 4
Coefficients C_1–C_3 for single rolling oscillation (panel A) and single pitching oscillation (panel B) at rib 5 and mid-rib 5 locations

X location	Coefficient C_1	Coefficient C_2	Coefficient C_3	Repeated flow region
Panel A				
6.6	8.006E1	−3.959E3	−6.727E5	Rib 5
7.17	1.331E2	−9.795E3	−3.047E5	Mid-rib 5
Panel B				
6.6	−2.099E1	1.116E4	−1.212E6	Rib 5
7.17	5.848E0	−2.956E4	1.371E7	Mid-rib 5

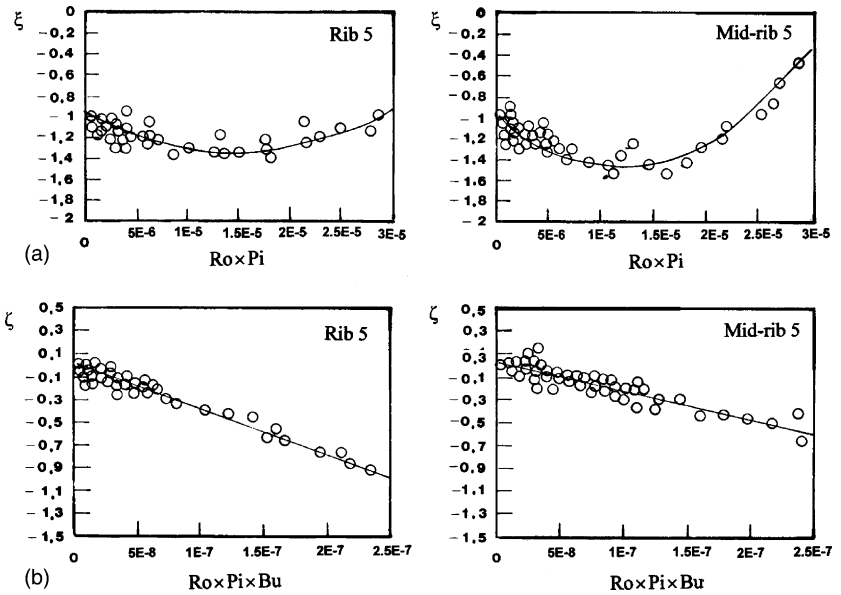

Fig. 9. Variations of ξ and ζ functions with rolling or pitching number at rib 5 and mid-rib 5 locations. Compound swinging oscillation (a) without and (b) with buoyancy interaction.

Table 5
Coefficients F_1 and F_2 for compound-mode swinging oscillation at rib 5 and mid-rib 5 locations

X location	$\xi = -1 + F_1(X) \times (\mathrm{Ro} \times \mathrm{Pi}) + F_2(X) \times (\mathrm{Ro} \times \mathrm{Pi})^2$		Repeated flow region
	$F_1(X)$	$F_2(X)$	
6.6	−5.205382E4	1.829861E9	Rib 5
7.17	−8.45387E4	3.517423E9	Mid-rib 5

Table 6
Coefficient G for compound-mode swinging oscillation at rib 5 and mid-rib 5 locations

X location	$\zeta = G(X) \times (\mathrm{Ro} \times \mathrm{Pi} \times \mathrm{Bu})$	Repeated flow region
	$G(X)$	
6.6	3.897132E6	Rib 5
7.17	2.401256E6	Mid-rib 5

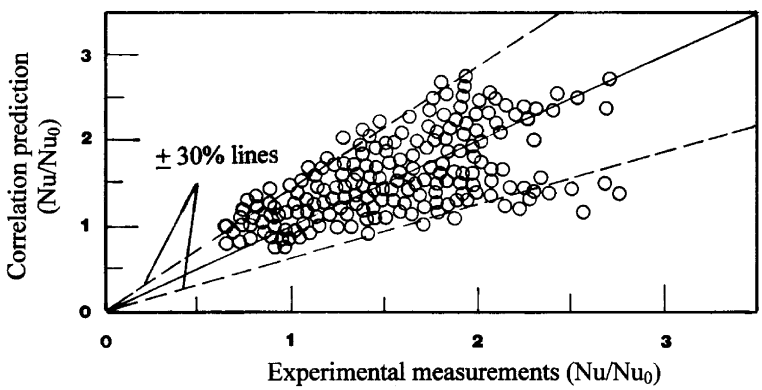

Fig. 10. Comparison of experimental measurements with correlation predictions.

±20% between the experimental and correlating results is achieved for 85% of the entire data generated.

5. Conclusions

This experimental study investigates the heat transfer inside a swinging rectangular channel with two opposite walls roughened by 45° staggered ribs. A detailed description of the heat transfer physics followed by a data correlating process, which complies with the physical constraints formulated from the experimentally based observations, describes the individual and interactive effects of the swinging forces and buoyancy, and the synergistic effects of harmonic and non-harmonic oscillations on heat transfer. As a result of the study the following salient points emerge:

1. The streamwise zigzag heat transfer variation with negligible buoyancy effect in the static channel along the centerline of rib-roughened surface is detected by the present arrangement of wall-temperature thermocouples. If the enhanced heat transfer factor is expressed as the ratio of the Nusselt number obtained in the rib-roughened rectangular channel to the Dittus–Boelter level [14], then the heat transfer with the test section static increases by a factor in the range of 3–5.6.

2. The swinging force effects complicated by buoyancy interaction with a greater influence attributing from the oscillation orientated across the narrow side of the rib-roughened rectangular channel cause heat transfer varying in the range of 0.75–2.5 times of the static channel value. The compound rolling and pitching force effects on heat transfer appear to be complex synergetic influences, but not additive, of two individual single-mode oscillating effects.

3. For single and compound modes of swinging oscillations with harmonic and non-harmonic rhythms, the *Re* variable effect on heat transfer could be reasonably uncoupled from swinging force effects by $Re^{B(Z)}$ relationship that considerably simplifies the quest of seeking for heat transfer correlation in a swinging channel.

4. The buoyancy interaction in a swinging channel could either improve or impede local heat transfer, which effect varies with the mode of swinging oscillation, the axial location and the values of rolling and pitching numbers. The reversal buoyancy effect from improving to impeding heat transfer is observed in the swinging channel subject to compound mode oscillation.

5. The extrapolating zero-buoyancy heat transfer data with single-mode swinging oscillation varies linearly with rolling or pitching numbers, which shows a streamwise reduction in the $\psi_{R,P}$ value. For single-mode rolling or pitching oscillation, the zero-buoyancy heat transfer data shows continuous improvement from the static level when rolling or pitching numbers increase up to about the fifth rib and mid-rib locations where the heat transfers are continuously decreased from the static references when the swinging force increases.

6. The zero-buoyancy synergistic effects with harmonic and non-harmonic swinging oscillations exhibit an initial heat transfer reduction from static references, which is followed by a tendency of heat transfer recovery when the value of $\mathrm{Ro} \times \mathrm{Pi}$ increases. With the synergistic compound swinging forces interacting with buoyancy, heat transfers are consistently reduced when $\mathrm{Ro} \times \mathrm{Pi} \times \mathrm{Bu}$ increases that unravels the impeding heat transfer effects.

7. A proposed heat transfer correlation, which is physically consistent, permits the individual and interactive effects of the forced convection, the single and compound modes of swinging forces with harmonic and non-harmonic rhythms and the buoyancy interaction on heat transfer in a rectangular rib-roughened channel to be taken into account.

References

[1] J.C. Han, J.S. Park, C.K. Lei, Heat transfer and pressure drop in blade cooling channels with turbulence promoters, NASA Contract Report NAG3-311, 1984, p. 138 (data sheet).

[2] T.M. Liou, J.J. Hwang, Turbulent heat transfer augmentation and friction in periodic fully developed channel flows, ASME J. Heat Transfer 114 (1992) 56–64.

[3] M.E. Taslim, T. Li, D.M. Kercher, Experimental heat transfer and friction in channels roughened with angled, V-shaped, and discrete ribs on two opposite walls, ASME J. Turbomach. 118 (1996) 20–28.

[4] J.R. Shen, Z. Wang, P.T. Ireland, T.V. Jones, A.R. Byerley, Heat transfer enhancement within a turbine blade cooling passage using ribs and combinations of ribs with film cooling holes, ASME J. Turbomach. 118 (1996) 428–434.

[5] B. Bonhoff, S. Parneix, B.V. Johnson, J. Schabacker, A. Bölcs, Experimental and numerical study of developed flow and heat transfer in coolant channels with 45 degree ribs, Int. J. Heat Fluid Flow 20 (1999) 311–319.

[6] B.V. Johnson, J.H. Wanger, G.D. Steuber, F.C. Yeh, Heat transfer in rotating serpentine passages with trips skewed to the flow, ASME J. Turbomach. 116 (1992) 113–123.

[7] S. Mochizuki, A. Murata, M. Fukunga, Effect of rib arrangements on pressure drop and heat transfer in a rib-roughened channel with a sharp 180 deg turn, ASME J. Turbomach. 119 (1997) 610–616.

[8] Y.J. Jang, H.C. Chen, J.C. Han, Flow and heat transfer in a rotating square channel with 45 deg angled ribs by Reynolds stress turbulence model, ASME J. Turbomach. 123 (2001) 124–131.

[9] S.W. Chang, Forced heat convection in a reciprocating duct fitted with 45 degree crossed ribs, Int. J. Thermal Sci. 41 (2002) 229–240.

[10] S.W. Chang, Y. Zheng, Enhanced heat transfer with swirl duct under rolling and pitching environment, J. Ship Res. 46 (2002) 149–166.
[11] A. Ivanova, V. Kozlov, D.V. Lyubimov, T. Lyubimova, Convective states in a fluid subjected to static gravity and non-translational oscillations, in: IX Eur. Symposium on Gravity Dependent Phenomena in Physical Science, Berlin, Abstracts, 1995, pp. 67–68.
[12] G.Z. Gershuni, D.V. Lyubimov, Thermal Vibrational Convection, John Wiley & Sons, 1998, pp. 344–354, ISBN 0 471 97385 8.
[13] Editorial Board of ASME Journal of Heat Transfer, Journal of heat transfer policy on reporting uncertainties in experimental measurements and results, ASME J. Heat Transfer 115 (1993) 5–6.
[14] F.W. Dittus, L.M.K. Boelter, University of California, Berkeley, CA, Publications in Engineering 2, 1930, p. 443.